interference. MIT was conducted by keeping the magnetic sensor on ground and then the UAV was flown at different heights from the sensor while recording magnetic data. A change of ~2 nT in magnetic data was observed when the UAV was flown at ~4 m and negligible change was found at more height than 4 m. No change in magnetic data is observed when the UAV was at a height of >6 m. Based on this experiment, a separation of 5 m between the UAV and magnetic sensor was found suitable, which has been further validated during flight.

An east–west trending dyke having a variable width of 50–100 m and strike length of several kilometres near Yacharam was chosen to test the UAV magnetometer along with ground magnetic survey. The dyke can be traced on either side of the Hyderabad–Nagarjuna Sagar road (on NH-65), 51 km from Hyderabad and 200 m north of Yacharam town. It is well exposed in the form of a geomorphic ridge at the test site and at places is covered by thin (<1 m) soil cover. The mafic dolerite dyke is a Proterozoic dyke intruding Neoarchean granite gneiss in a part of the Eastern Dharwar craton (Figure 1). In general, the area consists of several dykes of different orientations, size and ages. However, the Yacharam dyke is distinctly seen both in satellite images and on the ground, and therefore was chosen as the test area for the present study.

An area of 1 km × 0.6 km was selected as the test location with a N–S profile length of 900 m and line spacing of 50 m (Figure 2). Data were acquired at 5 samples/sec along 12 profile lines (L01 to L12), while the UAV was flown at a speed of 5 m/sec 35 m above the ground surface. Considering average topographic variations of about a metre over the study region, the height of the UAV was maintained at 35 m above the average height of the study area.

However, the UAV has an option of changing flight height during voyage and this can be planned at the starting time of flight. A ground magnetic survey was conducted along Line 02 prior to the drone magnetometer experiment for comparison of results. In addition, two lines, L02 and L04, were flown twice to test repeatability of data received from the UAV magnetometer. The standard deviation (SD) of repeat data along L02 and L04 was computed for 954 locations. The average SD for L02 was 3.09 nT and for L04 it was 2.39 nT. This would further improve with diurnal correction.

Figure 3 shows the data obtained from ground and UAV magnetic surveys along line L02. A good correlation with minor mismatch can be seen. This mismatch could be attributed to the GPS position accuracy in both surveys. The measurement repeatability test was conducted along two lines (L02 and L04) and the comparison indicates good correlation (Figure 4).

The data acquired by the UAV magnetometer experiment were processed through WinGLink software (Figure 5). It was observed that the intensity of contours trend in the E–W direction coinciding with the strike of the dolerite dyke. The contour pattern clearly reveals the dyke and adjacent granitic terrain. The contours are dense with high magnetic gradient over the dyke, while they are diffuse away from the dyke. The dyke is well reflected in the central part of the contour map derived from the UAV magnetic data of the study area (Figure 5). The results clearly distinguish the mafic dolerite dyke and granitic terrain in the test area. The present study has successfully demonstrated the capability of UAV-Magnetic survey, which is cost effective, faster and reliable.

1. Aleksandrov, D. and Penkov, I., In Proceedings of 8th International DAAAM Baltic Conference on Industrial Engineering, Tallinn, Estonia, 19–21 April 2012.
2. Samal, A. K., Srivastava, R. K. and Sinha, L. K., *J. Earth Syst. Sci*., 2015, **124**(5), 1075–1084.

ACKNOWLEDGEMENTS. We thank the Council of Scientific and Industrial Research, New Delhi for funding a project (DREAM) under mission mode scheme and Jitendra J. Jadhav (Director, CSIR-National Aerospace Laboratories, Bengaluru) for constant guidance during the development of the UAV. We also thank P. S. Goel (Chairman, CSIR-NGRI Research Council and Monitoring Committee for the DREAM project) for his guidance and constructive suggestions, and T. R. K. Chetty (formerly at CSIR-NGRI) for geological information.

Received 1 January 2020; revised accepted 22 June 2020

G. ASHOK BABU[1]
G. VAMSI KRISHNA[1]
V. M. TIWARI[1,*]
R. ANTONY[2]
C. S. SURAJ[2]
K. T. VIKAS[2]
P. V. S. MURTHY[2]

[1]*CSIR-National Geophysical Research Institute, Hyderabad 500 007, India*
[2]*CSIR-National Aerospace Laboratories, Bengaluru 560 017, India*
**For correspondence.*
e-mail: vmtiwari@ngri.res.in

Unique polyphase deformational structures of Lunawada metasedimentary rocks identified from remote sensing imagery

The Mesoproterozoic metasedimentary rocks of the Lunawada Group in the Aravallis, northern Gujarat, India, exhibit unique and spectacular outcrops of deformation structures in mesoscale[1]. Here we present an analysis of imagery from Sentinel-2 earth observation satellite (courtesy: European Space Agency) to identify an array of unique deformational 'meso' structures from brittle–ductile regime[2,3], which indicates polyphase deformation over an area of approximately 70 km^2. The array of deformation structures in mesoscale also makes it a pertinent candidate 'geosite' for researchers of structural geology, graduate and postgraduate students and geology enthusiasts.

The Lunawada Group is mostly constituted of quartzite and metapellites[4–6]. The microstructural evidences of deformation in these rocks have been studied in details[7–9]. Quartzites occur as high ridges, whereas brown schist forms

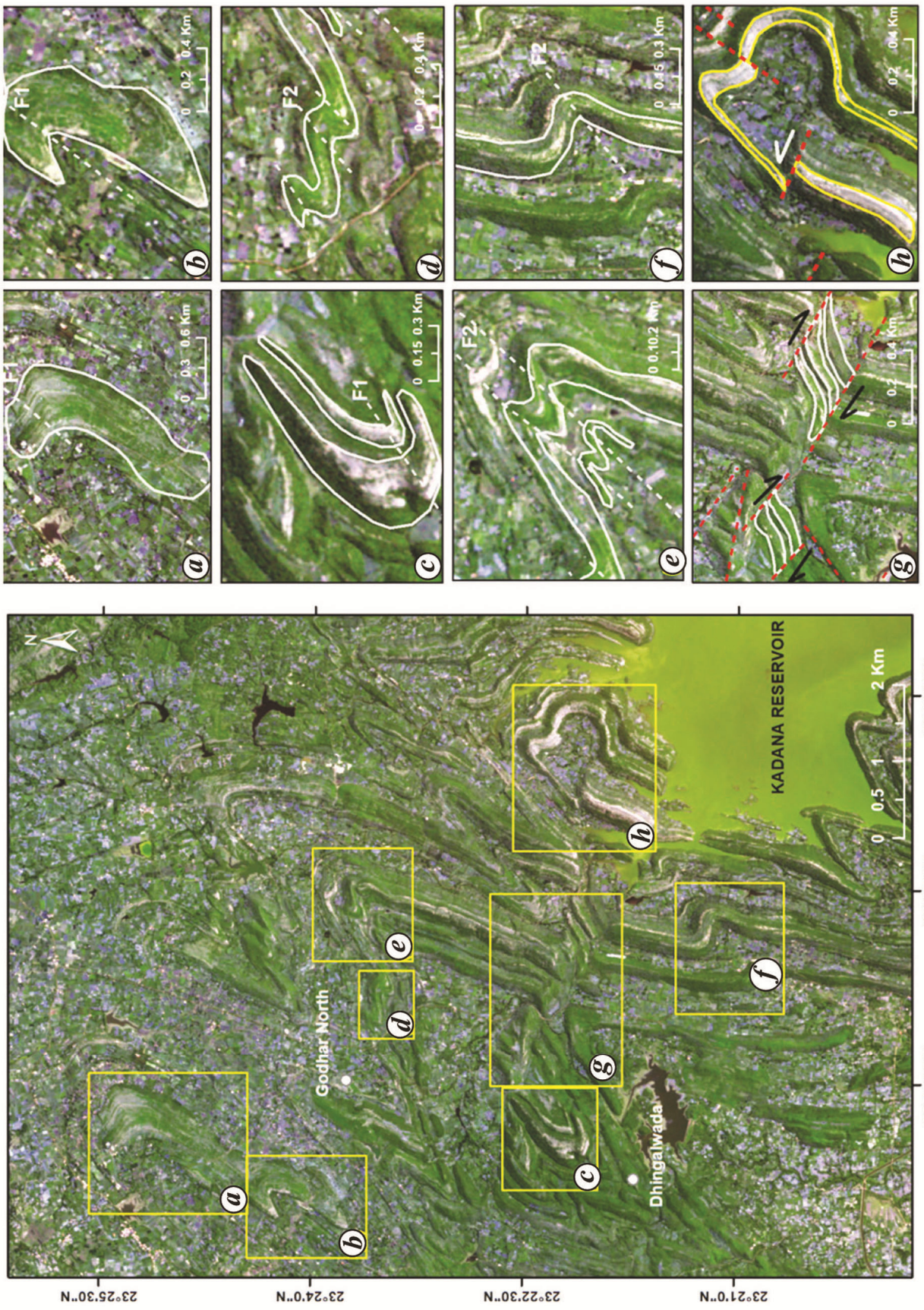

Figure 1. Synoptic view of quartzite–schist exposures of the Lunawada group in Gujarat, India, as seen from Sentinel-2 satellite imagery (true colour composite: bands 4-3-2). (Inset) ***a–c***, 'Root-less' folds; ***d***, Z-folds; ***e***, M-fold; ***f***, S-fold; ***g***, S–C structure; ***h***, Flanking structure (white dotted lines denote fold axis; red dashed lines denote faults/fractures).

Table 1. Sentinel-2 multispectral instrument band specifications

Sentinel-2 bands	Central wavelength (μm)	Resolution (m)
Band 1 – Coastal aerosol	0.443	60
Band 2 – Blue	0.490	10
Band 3 – Green	0.560	10
Band 4 – Red	0.665	10
Band 5 – Vegetation red edge	0.705	20
Band 6 – Vegetation red edge	0.740	20
Band 7 – Vegetation red edge	0.783	20
Band 8 – NIR	0.842	10
Band 8A – Vegetation red edge	0.865	20
Band 9 – Water vapour	0.945	60
Band 10 – SWIR – Cirrius	1.375	60
Band 11 – SWIR	1.610	20
Band 12 – SWIR	2.190	20

low-lying subdued topography. The Lunawada rocks have been subjected to upper greenschist to amphibolite facies metaphorphism[10,11]. This topographical variation makes the rocks discernible from remotely sensed satellite imagery. Further, the satellite imagery also provides a synoptic view of the entire region, thereby enabling identification of the mesoscale structures in order of ~500 m to 2 km, which otherwise is difficult to visualize in an inter relatable manner during field traverses.

The Sentinel-2 satellite acquires images of the earth in the visible (V) and near-infrared (NIR) to the shortwave infrared (SWIR) regions of the electromagnetic spectrum (Table 1)[12]. Of these, the three RGB bands (blue (~493 nm), green (560 nm), and red (~665 nm)) and NIR band (~833 nm) are acquired in 10 m ground resolution, with a swath of 290 km, making the imagery pertinent for regional geological studies. We have downloaded the Level 1C imagery from Copernicus Open Access Hub (previously known as Sentinels Scientific Data Hub; source: https://scihub.copernicus.eu/) in GeoTIFF format[12]. The Level-1C processing includes radiometric and geometric corrections along with orthorectification to generate highly accurate geolocated products (12.5 m at 95.5% confidence)[12]. The image has been further processed using standard contrast stretching algorithms (e.g. histogram stretch) and then stacked in multibands (band 4: band 3: band 2 = red: green: blue), thus generating a true colour composite image of the region for analysis.

A synoptic view of the region, as seen from the satellite imagery, is given in Figure 1, with the individual structures annotated in 1 : 25,000–1 : 50,000 scale (inset, Figure 1 *a–f*). 'Rootless' intrafolial folds are tight isoclinal to overturned folds resulting from synchronous shear[2,13–15]. In this region, a number of such intrafolial folds are developed within the quartzite layer (Figure 1 *a–c*). In addition, the folded quartzite ridges show Z-fold (Figure 1 *d*), M-fold (Figure 1 *e*) and S-fold (Figure 1 *f*) geometries.

Along with the folded geometries, brittle–ductile structures are manifested in the region in mesoscale. Possible S–C structure (Figure 1 *g*) and flanking structure/fold (Figure 1 *g*) are observed to be manifested by the quartzite and metapelite bands. The S–C structure was first described by Lister and Snoke[16] in microscale. However, occurrence of the same in the meso- to megascale is a rarity. Herein, a possible mesoscale S–C structure is defined within the folded quartzite–metapelite rocks (vergence towards SE)[2,13]. The folded quartzite bands are sheared from the top to SE, attributed by the sub-parallel S structures, which transect at an angle to the C fracture planes, along NW–SE (Figure 1 *g*). Later, the S–C structure is dislocated by a fault.

Flanking structures (or flanking folds) in shear zones were first reported by Passchier[17] and subsequently studied in detail by others[13,14,18–21]. We observe that the quartzite bands have had undergone poly-phase folding and subsequently the fold limbs are offset by faults, exhibiting a possible mesoscale flanking structure (Figure 1 *h*). The host element (HE) of the flanking structure is defined by quartzite layers with the cross-cutting element (CE) being the fracture plane. HE shows sinistral displacement across CE. From a combination of slip direction and drag of host element, the flanking structure may be classified as 'reverse A type' flanking fold (according to figure 2 of Exner *et al.*[22]).

Minimum three deformation events have been reported within the rocks of the Lunawada Group in this area[1,11]. Synoptic view provided by the imagery supports these observations. The first deformation (D1) produced regional schistosity forming mica schist and quartzite bands parallel to the schistosity. This also resulted in the dominant NNE–SSW to NE–SW trending folds (F1). The second deformation (D2) phase may have obliterated or modified the imprints of older folds (resulting in the occurrence of the 'rootless' intrafolial folds) and led to folding of the limbs of F1 (thus forming F2). Axial trace of F1 folds are co-trending to F2, and hence are co-axial. A possible non-coaxial nature of the third deformation (D3) resulted in NW–SE faults/fractures with S–C structures and flanking fold defined by the fold limbs.

The region falls north of Lunawada village, left embankment of Kadana reservoir in Gujarat. It is bounded by 23°20′50.10″N–23°25′39.70″N lat. and 73°44′42.04″E–73°50′39.14″E long. Further analysis of synoptic satellite imagery reveals significant information about fold geometries, brittle–ductile deformation structures and their interrelations.

1. Joshi, A., Limaye, M. A. and Deota, B. S., *Gondwana Geol. Mag.*, 2013, 53–56.
2. Mukherjee, S., *Deformation Microstructures in Rocks*, Springer Geochemistry/Mineralogy, Berlin, Germany, 2013, pp. 1–111; ISBN 978-3-642-25608-0.
3. Mukherjee, S., *Geol. Mag.*, 2014, **151**(6), 957–974.
4. Daru, N. D., A report on geological mapping of Kadana, Sant, Lunawada and Dungarpur States. Unpub. Report. Geol. Surv. India, 1915.
5. Gupta, B. C. and Mukherjee, P. N., *Rec. Geol. Surv. India*, 1938, **73**, 163–208.
6. Iqbaluddin and Venkataramaiah, T., Photogeological mapping with selective checks in parts of Kadana reservoir area, Panchmahals district, Gujarat. Unpub., Report, Geol. Surv. India, 1976.
7. Mamtani, M. A. and Karanth, R. V., *Curr. Sci.*, 1996, **70**, 396–399.
8. Mamtani, M. A. and Karanth, R. V., *J. Geol. Soc. India*, 1997, **50**, 171–178.
9. Mamtani, M. A., Karanth, R. V. and Greiling, R. O., *J. Struct. Geol.*, 1999, **21**, 711–718.

10. Mamtani, M. A., Karanth, R. V., Merh, S. S. and Greiling, R. O., *Gondwana Res.*, 2000, **3**, 175–187.
11. Mamtani, M. A., Merh, S. S., Karanth, R. V. and Greiling, R. O., *J. Asia Earth Sci.*, 2001, **19**, 195–205.
12. https://sentinel.esa.int/web/sentinel/user-guides/sentinel-2-msi
13. Mukherjee, S., *Atlas of Shear Zone Structures in Meso-Scale*, Springer Geology, Berlin, Germany, 2014, pp. 1–124; ISBN 978-3-319-0088-6.
14. Mukherjee, S., *Atlas of Structural Geology*, Elsevier, Amsterdam, The Netherlands, 2015.
15. Joshi, A., Limaye, M. A. and Deota, B. S., *Int. J. Earth Sci.*, 2018, **108**(1), 183–186.
16. Lister, G. S. and Snoke, A. W., *J. Struct. Geol.*, 1984, **6**(6), 617–638.
17. Passchier, C. W., *J. Struct. Geol.*, 2001, **23**(6), 951–962.
18. Grasemann, B., Stüwe, K. and Vannay, J. C., *J. Struct. Geol.*, 2003, **25**(1), 19–34.
19. Mukherjee, S. and Koyi, H. A., *Geol. Mag.*, 2009, **146**, 517–526.
20. Mukherjee, S., *YES Bull.*, 2011, **1**, 21–29.
21. Biswas, A. and Roy, P., *Int. J. Earth Sci.*, 2018, **107**, 167–168.
22. Exner, U., Mancktelow, N. S. and Grasemann, B., *J. Struct. Geol.*, 2004, **26**(12), 2191–2201.

ACKNOWLEDGEMENTS. We thank Dr S. Mukherjee (Department of Earth Sciences, IIT Bombay) for useful comments and suggestions. We also thank Prof. M. Mamtani (Department of Geology and Geophysics, IIT Kharagpur) for his comments on the initial version of this paper.

Received 21 April 2020; revised accepted 1 July 2020

PRIYOM ROY[1,*]
ANKITA BISWAS[2]

[1]*National Remote Sensing Centre, Indian Space Research Organisation,*
[2]*Geological Survey of India, Hyderabad 500 068, India*
**For correspondence.*
e-mail: roy.priyom@gmail.com

Uranium and associated polymetallic mineralization in Palaeoproterozoic Khetabari Formation of Bomdila Group, Laggi Gamlin area, West Siang district, Arunachal Pradesh, India

Palaeoproterozoic Khetabari Formation of Bomdila Group in Arunachal Pradesh, India is an N–S to NE–SW trending volcano-sedimentary sequence. It stratigraphically overlies the Se La Group and is exposed in the western limb of Siang antiform (Figure 1 *a*). The Khetabari Formation comprises calc–silicate rocks/marble, carbonaceous phyllite, magnetite quartzite, quartzite/schistose quartzite and mica schist (Figure 1 *b* and *c*) with some concordant and discordant basic intrusions. It is thrusted over the Palaeoproterozoic Tenga Formation in the eastern margin[1]. Intrusive Ziro granite gneiss (1536–1914 Ma) is exposed along its western margin[2]. Multiple episodes of deformation have affected the Khetabari Formation. F1 folds well-preserved in massive and schistose quartzites, show tight to isoclinal, reclined to recumbent geometry and their axial planes generally show N–S to NNE–SSW strike. The most pervasive planar fabric S1 is developed parallel to the axial plane of the F1 folds, and is predominantly parallel to the S0 plane. The F2 folds have coaxially refolded the axial planes of F1 folds giving rise to type-III interference patterns. Crenulation cleavage (S2) is related to F2 folding. Steeply plunging, inclined, open folds of the third generation superposed on earlier folds have N–S axial planes. N–S to NNE–SSW trending fault has given rise to fault breccia. Sigmoidal magnetite grains indicate sinistral shearing. In the shear zones, elongated quartz grains and S–C fabrics are noted. These structures have played a vital role in the circulation of mineralizing fluids in the Khetabari Formation, and have served as locales for uranium and associated polymetallic mineralization (Figure 2 *a* and *b*).

Exploration efforts over the last few decades in Arunachal Pradesh by the Atomic Minerals Directorate for Exploration and Research, Shillong have resulted in locating several uranium and associated polymetallic occurrences in the Khetabari Formation. Sie Rimi-Noko-Lete Nala[3,4], Gamkak-Tapeyor[5] and Kau Nala[6] are a few examples. They demonstrate the importance of structurally controlled uranium and associated polymetallic mineralization in the Khetabari Formation. Subsurface exploration at Noko Nala–Kardo–Badak area has established subsurface continuity of uranium mineralization in magnetite–calcite schist over a strike length of 1200 m with grade up to 0.036 %eU_3O_8 and thickness up to 8.1 m (ref. 4).

Here we provide details of recently located uranium and associated sulphide mineralization in a breccia zone (Laggi Gamlin-1; LGM-1) and in sheared magnetite quartzite (Laggi Gamlin-2; LGM-2) at Laggi Gamlin, West Siang district, Arunachal Pradesh (Figure 1).

The uranium mineralization of LGM-1 is hosted by breccia and is located in the first-order creek section about 900 m SSW of Laggi Gamlin village. The 1–10 m wide mineralization zone here is traced along the N–S strike over a length of 150 m. The strike coincides with the axial plane strike of F3 folds in the area. The breccia consists of few millimetres to more than 5 cm-sized calcite clasts cemented by ferruginous matter (Figure 2 *a*). The study reveals that ferruginous cement is radioactive. Thirteen samples of ferruginous breccia have assayed 0.009–0.027 (av. 0.012) %U_3O_8 and <0.005% ThO_2.

Petromineralogical study shows that breccia has developed from precursor calc–silicate rock/marble. It has angular clasts of calcitic marble which are cemented by a matrix composed of magnetite, hematite, K-feldspar and quartz (Figure 3 *a*). Accessory minerals are pyrite, chalcopyrite and rutile. Uranium occurs in the adsorbed state in magnetite and hematite in the matrix/cement of the brecciated marble.

The LGM-2 uranium mineralization is in sheared magnetite quartzite. Uranium